ChemElectroChem

Research Article
doi.org/10.1002/celc.202300479

Chemistry Europe
European Chemical Societies Publishing

www.chemelectrochem.org

VIP *Very Important Paper*

NIR-emitting Electrochromic Windows for Cold Climate Region Buildings

Daniela Pinheiro,*[a, f] Mariana Fernandes,[a] Rui F. P. Pereira,[b] Sónia Pereira,[c] Sandra F. H. Correia,[d] M. Manuela Silva,[b] Elvira Fortunato,[c] Rute A. S. Ferreira,[e] Maria Cristina Gonçalves,[a] and Verónica de Zea Bermudez*[a]

Electrochromic devices (ECDs) comprising visible/near-infrared (NIR) transparent amorphous indium zinc oxide (a-IZO) outermost layers and novel NIR-emitting electrolytes are proposed for smart windows of buildings in cold climate regions. The electrolytes are composed of a di-urethane cross-linked poly(oxyethylene)(POE)/siloxane hybrid matrix (d-Ut(600), 600 is the average molecular weight of the POE chains in $gmol^{-1}$), 1-butyl-3-methylimidazolium chloride ionic liquid, and the Er-$(tta)_3(H_2O)_2$ complex (tta^- is 2-thenoyltrifluoracetonate). The electrolytes, synthesized by sol-gel route, were obtained as transparent, flexible, and hydrophilic monoliths with nanoscale surface roughness, exhibiting emission in the NIR wavelength region. The first electro-optical tests, performed in 2019, with an archetypal ECD including amorphous tungsten oxide and crystalline nickel oxide as EC layers, a-IZO as outermost layers, and d-Ut$(600)_{400}$Er$(tta)_3(H_2O)_2$[Bmim]Cl (400 is the molar ratio of oxyethylene units/Er^{3+} ion) as the electrolyte, demonstrated rather low coloration efficiency (CE_{in}/CE_{out}) values of $-4/+6\ cm^2C^{-1}$ at 555 nm. After 3 years of storage at rest in the dark and at room temperature, the same device demonstrates a huge performance enhancement, leading to CE_{in}/CE_{out} values about two orders of magnitude higher, apart from higher optical density, and improved cycling stability. In addition, this device offers a bright hot, and semi-bright warm dual modulation operation suitable for smart windows of skylights, roof lights, upper windows, inclined glazing, and privacy glazing of buildings located in cold climate regions.

Introduction

Economic progress and increasing population are driving the energy demand which is mainly generated from fossil fuels. However, these resources are limited and have substantial deleterious environmental impacts (global warming and climate change). The European Climate Law determines that the European Union economy and society should become climate-neutral by 2050 in a socially fair and cost-efficient manner.[1]

The building sector is particularly critical, representing 30–40% of the primary energy worldwide.[2] Temperature control inside the buildings is one of the most critical factors that contribute to the increase of energy consumption in buildings. The Sustainable Development Goals 7, 11, and 13 of the 2030 Sustainable Development Agenda[3] aim at developing energy-efficient buildings for a thriving, sustainable, climate-neutral, resilient, safe, and healthy society.

Innovative research plays a pivotal role in the transition to more efficient, greener, sustainable, and safe energy solutions.[4] "Smart windows" based on electrochromic devices (ECDs) are of utmost interest for the implementation of zero-energy buildings (ZEBs). This promising technology enables the control of the visible and near-infrared (NIR) spectral regions of the solar spectrum through the application of a small electric voltage (normally lower than 3.0 V), reducing the energy consumption of buildings up to 30%.[5] In the last years, several organic and inorganic materials, such as conducting polymers,[5a,6] transition metal oxides,[7] and viologen,[8] among others, have been widely explored as active EC materials in ECDs. The electrolyte is another fundamental constituent of the ECD.

[a] *Dr. D. Pinheiro, Dr. M. Fernandes, Prof. Dr. M. C. Gonçalves, Prof. Dr. V. de Zea Bermudez*
Chemistry Department and CQ-VR
University of Trás-os-Montes e Alto Douro
5000-801 Vila Real (Portugal)
E-mail: danielap@utad.pt
vbermude@utad.pt

[b] *Dr. R. F. P. Pereira, Prof. Dr. M. M. Silva*
Chemistry Department and Centre of Chemistry
University of Minho
4710-057 Braga (Portugal)

[c] *Dr. S. Pereira, Prof. Dr. E. Fortunato*
CENIMAT/I3N, Departamento de Ciência dos Materiais
Faculdade de Ciências e Tecnologia
2829-516 Lisboa (Portugal)

[d] *Dr. S. F. H. Correia*
Instituto de Telecomunicações and
University of Aveiro
3810-193 Aveiro (Portugal)

[e] *Prof. Dr. R. A. S. Ferreira*
Physics Department and CICECO-Aveiro Institute of Materials
University of Aveiro
3810-193 Aveiro (Portugal)

[f] *Dr. D. Pinheiro*
Present address:
CPIRN-IPG – Center of Potential and Innovation of Natural Resources
Polytechnic of Guarda
6300-559 Guarda (Portugal)

Supporting information for this article is available on the WWW under https://doi.org/10.1002/celc.202300479

In this work, a new NIR-emitting electrolyte was synthesized and used to produce classical 5-layer configuration ECDs meant to operate in the windows of buildings situated in a cold climate region. This device should, not only enable the control of the incoming solar visible and NIR radiation but also be able to emit in the NIR to provide additional indoor thermal comfort. The device comprised transparent conductive oxide (TCO) outermost layers of amorphous indium zinc oxide (a-IZO), which are transparent in the visible/NIR spectral regions,[9] and complementary amorphous tungsten oxide (a-WO_3) and crystalline nickel oxide (c-NiO) EC layers. Ideally, such devices are expected to provide, apart from energy savings, increased visual and thermal comfort to the occupants of the ZEBs of the future smart cities. Using sol-gel chemistry, a novel di-urethane cross-linked poly(oxyethylene) (POE)/silica matrix (di-urethanesil, noted as d-Ut(600)[10]) electrolyte doped with the bisaquatris(thenoyltrifluoroacetonate) erbium(III) (Er-$(tta)_3(H_2O)_2$)[11] complex and the 1-butyl-3-methylimidazolium chloride ([Bmim]Cl) ionic liquid (IL) was synthesized. For comparison purposes, an electrolyte lacking IL was also synthesized.

The rationale for the electrolyte synthesis and design was the following. The versatile sol-gel route is among the most attractive methods for the fabrication of electrolytes to be included in ECDs.[12] Among the sol-gel derived organically modified silicate electrolytes (ormolytes) reported in the literature, the attractiveness of the di-urea and di-urethane cross-linked POE/siloxane (di-ureasils and di-urethanesils) host hybrid matrices (noted as d-U(Y) and d-Ut(Y'), respectively, where Y and Y' represent the average molecular weight of the POE chains) doped with alkaline and lanthanide salts, ILs, lanthanide (Ln^{3+}) complexes, or their mixtures, have been extensively highlighted by some of us.[10a,11–13] As far as the doping agents are concerned, the IL and the Er^{3+} complex were chosen in the present case to impart high ionic conductivity and NIR emission, respectively.

ILs, as room-temperature liquid electrolytes, exhibit exceptional properties for the electrochemical field, such as enhanced ionic conductivity, high thermal and redox stability and broad electrochemical potential window, thus offering innumerous advantages for ECDs technology.[5c,13a,14] Recent studies showed that the inclusion of [Bmim]Cl in the di-ureasil and di-urethanesil electrolytes improved significantly the levels of ionic conductivity.[10a,13a] [Bmim]Cl is particularly suitable for eco-friendly energy applications[15] given its: (i) very low toxicity,[16] (ii) reversible thermotropic effect at *ca.* 30 °C[17] and, (iii) strong hydrogen bond–accepting ability.[18]

As to the use of Ln^{3+} complexes, they are particularly appealing, since they exhibit unique photophysical features, including high luminescence quantum yield, high luminescence lifetimes, tunable emission spectral range (UV/visible/NIR), and ligand-dependent luminescence sensitization (antenna effect).[19] This effect enables Ln^{3+} complexes to absorb light in the UV region and emit light in the visible (*e.g.*, Eu^{3+} and Tb^{3+}) and NIR (*e.g.*, Er^{3+} and Nd^{3+}) spectral regions.[20] Previous studies demonstrated that materials doped with Er^{3+} complexes have a great potential for electro-optics.[11,21] The addition of the $Er(tta)_3(H_2O)_2$ aquocomplex to the d-Ut(600) matrix looked quite attractive. It was demonstrated that the addition of Eu^{3+} ions as the $Eu(tta)_3(H_2O)_2$ complex to di-urethanesil[22] or di-ureasil[23] networks led to a significant enhancement of the quantum efficiency. This effect was associated with the replacement of water molecules in the Eu^{3+} first-coordination sphere of the $Eu(tta)_3(H_2O)_2$ complex by oxygen atoms of the carbonyl groups of the urethane or urea groups of the di-urethanesil or di-ureasil hosts, respectively, which decreased the non-radiative pathways for de-excitation of the emissive state, increasing the radiative ones. Electrolytes composed of $[Bmim]^+$-based ionosilicas including anionic lanthanide complexes $[Ln(tta)_4]^-$ and the IL 1-butyl-3-methylimidazolium hexafluorophosphate ([Bmim][PF_6]) were proposed very recently.[24] The present system is, thus, our first investigation of a hybrid electrolyte comprising a mixture of a Ln^{3+} complex and an IL, aiming the development of heat generation ECDs.

The primary goal of this work was to characterize the new electrolytes, and evaluate the electro-optical performance of the assembled glass/a-IZO/a-WO_3/electrolyte/c-NiO/a-IZO/glass devices (Figure 1). An ECD devoid of IL was also tested. The second purpose of the present work was to study how time affects the operation of such a device after a long period of storage at rest. The results reported demonstrate that this procedure had a beneficial rejuvenation influence, opening the avenue for applications other than windows where operation is required upon demand after long rest.

Results and Discussion

Physical-chemical characterization

The electrolyte is a fundamental component of the ECD. It should exhibit very low electronic conductivity, high ion diffusion to guarantee fast kinetics, transparency, no leakage or glass buckling risks, and good adhesion to the electrodes. A thorough physical-chemical examination of the electrolyte must always include the analysis of the microstructure and wettability behaviour since these parameters may affect the operation of the ECD and thus the coloration efficiency (CE).

In the present work the structure, morphology and surface properties of the d-Ut$(600)_{400}$Er$(tta)_3(H_2O)_2$ and d-Ut$(600)_{400}$Er-$(tta)_3(H_2O)_2$[Bmim]Cl electrolytes were analyzed. The results of this characterization study of the electrolyte materials may be found in the Supporting Information (SI). Valuable information regarding the strength and extension of hydrogen bonding in the d-Ut$(600)_{400}$Er$(tta)_3(H_2O)_2$ and d-Ut$(600)_{400}$Er-$(tta)_3(H_2O)_2$[Bmim]Cl electrolytes with respect to the situation in d-Ut$(600)_\infty$ was retrieved from the Attenuated Total Reflection Fourier Transform infrared (ATR-FTIR) spectra (Figures S1 and S2). The texture of the samples was studied by Scanning Electronic Microscopy (SEM) (Figures S3, S4 and S5) and Atomic Force Microscopy (AFM) (Figure S6 and Table S1). The static water contact angle (CA) and surface free energy (SFE) values

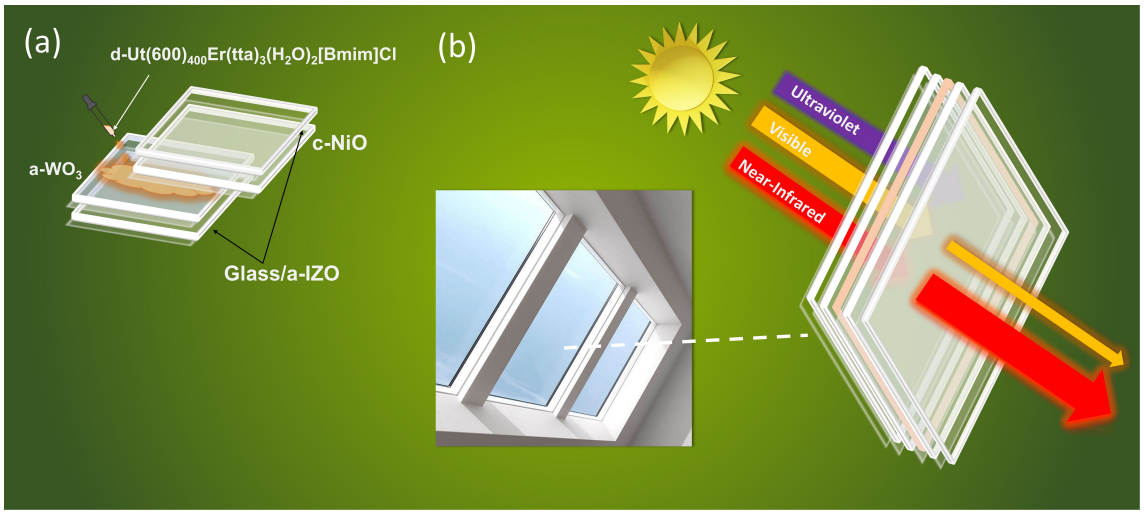

Figure 1. Schematic representation of the glass/a-IZO/a-WO_3/d-Ut(600)$_{400}$Er(tta)$_3$(H_2O)$_2$[Bmim]Cl/c-NiO/a-IZO/glass ECD configuration (a), and illustration of the operation mode of the assembled ECD (b).

were calculated for both films (Figure S7) and the wetting envelopes deduced (Figure S8).

Ionic conductivity

The variation of the ionic conductivity of d-Ut(600)$_{400}$Er(tta)$_3$(H_2O)$_2$ and d-Ut(600)$_{400}$Er(tta)$_3$(H_2O)$_2$[Bmim]Cl with temperature is depicted in Figure 2a. The non-linear variation observed is characteristic of disordered electrolytes. This Arrhenius plot allows concluding that the ionic conductivity of d-Ut(600)$_{400}$Er(tta)$_3$(H_2O)$_2$[Bmim]Cl at room temperature (4.68×10^{-5} S cm^{-1}) (Figure 2a, purple line and symbols) is about 3 orders of magnitude higher than that of d-Ut(600)$_{400}$Er(tta)$_3$(H_2O)$_2$ (1.80×10^{-8} S cm^{-1}) (Figure 2a, green line and symbols) and d-Ut(600)$_\infty$ (1.80×10^{-8} S cm^{-1} at 21 °C[10a]). At 100 °C d-Ut(600)$_{400}$Er(tta)$_3$(H_2O)$_2$[Bmim]Cl (Figure 2a, purple line and symbols) achieved the highest ionic conductivity (3.54×10^{-4} S cm^{-1}). From these findings, it is clear that the addition of the [Bmim]Cl IL to the electrolyte formulation was quite beneficial. For both samples an increase of temperature led to an ionic conductivity enhancement. This effect may be correlated with an increase of free volume, polymer segmental mobility, and charge mobility.[10a]

Figures 2b and 2c show the Nyquist plots for d-Ut(600)$_{400}$Er(tta)$_3$(H_2O)$_2$ and d-Ut(600)$_{400}$Er(tta)$_3$(H_2O)$_2$[Bmim]Cl, respectively, within the temperature range analyzed. The Nyquist plots for d-Ut(600)$_{400}$Er(tta)$_3$(H_2O)$_2$ are composed of a semicircle at high frequency and a straight line at low frequencies (Figure 2b), whereas those for d-Ut(600)$_{400}$Er(tta)$_3$(H_2O)$_2$[Bmim]Cl show straight lines over the whole frequency range (Figure 2c).[25] The semicircle is associated with the charge transfer process, and the straight lines are attributed to the diffusion process, *i.e.*, with the electrolyte/electrode interface.[10a] The origin of the ionic conductivity in the electrolytes is unknown at present, but given the major increase observed upon the introduction of the IL we feel tempted to speculate that protons are probably the main charge carriers.

Photoluminescence studies

Figure 3a compares the emission spectra of Er(tta)$_3$(H_2O)$_2$ (black line), d-Ut(600)$_{400}$Er(tta)$_3$(H_2O)$_2$ (red line) and d-Ut(600)$_{400}$Er(tta)$_3$(H_2O)$_2$[Bmim]Cl (blue line) in the NIR spectral range revealing the intra-4f^{11} transition ($^4I_{13/2}\rightarrow{}^4I_{15/2}$) of the Er^{3+} ions around 1530 nm.

After the incorporation into the hybrid host, the spectra became narrower and a series of Stark components are discerned (dashed vertical lines, Figure 3a), corroborating changes in the Er^{3+} local environment similar to the situation found for the analogous Eu^{3+} aquocomplex.[22,23]

Under UV excitation, a broad band in the visible range is also noticed (Figure 3b). The band in the spectra of d-Ut(600)$_{400}$Er(tta)$_3$(H_2O)$_2$ (red line) and d- Ut(600)$_{400}$Er(tta)$_3$(H_2O)$_2$[Bmim]Cl (blue line) are alike, peaking in the blue spectral region around 410 nm, despite a blue-shift around 5 nm. This band is blue-shifted compared to that in the isolated complex, whose emission in the visible reveals a broad band around 420 nm (black line), resembling that already reported for the Eu^{3+} isostructural complex which was attributed to the triplet states of the tta^- ligands.[26] The fact that this broad band is independent of the excitation wavelength (Figures S9–S11) provides additional evidence that it is dominated by the ligands, as the hybrid host intrinsic emission typically red-shifts as the excitation wavelengths increases.[27]

The excitation spectra (Figure 3c) revealed a broad band (fwhm ~1100 nm) in the UV/blue spectral region (300–450 nm) ascribed the tta^- triplet states.[23] There is a narrowing of the broadband in the spectra of d-Ut(600)$_{400}$Er(tta)$_3$(H_2O)$_2$[Bmim]Cl compared to that of the Er(tta)$_3$(H_2O)$_2$ complex (Figure S12) reinforcing that the Er^{3+}-local environment was modified,

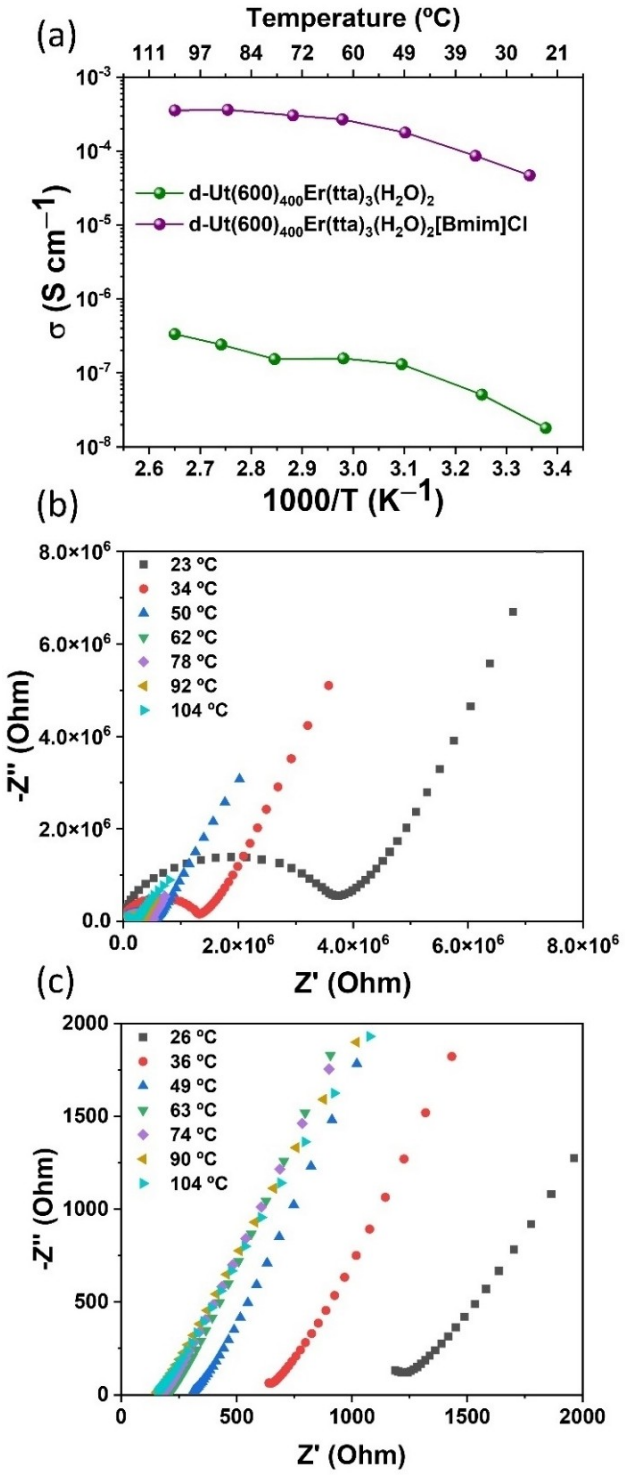

Figure 2. (a) Ionic conductivity of d-Ut(600)$_{400}$Er(tta)$_3$(H$_2$O)$_2$ (green line and symbols) and d-Ut(600)$_{400}$Er(tta)$_3$(H$_2$O)$_2$[Bmim]Cl (purple line and symbols) as a fraction of the reciprocal temperature. The lines are guidelines for the eye. Nyquist plots for (b) d-Ut(600)$_{400}$Er(tta)$_3$(H$_2$O)$_2$ and (c) d-Ut(600)$_{400}$Er(tta)$_3$(H$_2$O)$_2$[Bmim]Cl.

whereas there are no significant differences concerning this aspect for d-Ut(600)$_{400}$Er(tta)$_3$(H$_2$O)$_2$. Moreover, the broad band is overlapped by a series on intra-4f[11] lines, whose relative intensity decreases when the complex is incorporated into the host, suggesting a better shielding of the Er^{3+} ions and a more efficient ligands-to-Er^{3+} energy transfer process. The excitation spectra monitored in the visible spectral range are shown in Figures S13–S15.

To quantify the optical features of the electrolytes, the absolute emission quantum yield values excited in the UV were calculated. For the isolated complex, the value lies beyond the detection limits of the experimental apparatus (>0.001). Upon incorporating it into the di-urethanesil (d-Ut(600)$_{400}$Er(tta)$_3$(H$_2$O)$_2$), the quantum yield increased to 0.02, giving support to the explanation that, in the hybrid, oxygen atoms of the carbonyl groups of the urethane linkages of d-Ut(600) replaced labile water molecules of the 1st coordinating shell of Er^{3+}, thus contributing to the decrease of non-radiative channels. Nonetheless, the addition of the IL (d-Ut(600)$_{400}$Er(tta)$_3$(H$_2$O)$_2$[Bmim]Cl) yielded a reduction in the quantum yield (<0.001). This fact suggests the existence of extra-nonradiative channels associated with the organic ligands of the IL.

Evaluation of the performance of the prototype ECDs

Right after its assembly back in july 2019, the ECD@Er[Bmim]Cl device was subjected to the following steps: (1) 20 chronoamperometry (CA) cycles (±1.5 V, 50 s), (2) 6 cyclic voltammetry (CV) cycles at 20 mV s^{-1} (±2.0 V), and (3) 20 CA cycles (±2.0 V, 50 s). The transmittance (T) values obtained at 555 nm for +2.0/−2.0 V in the three following CA time interval cycles (Table 1 and Figure S16) were: 78/69% (I), 82/65% (II) and 67/57% (III). The ECD device showed good cycling stability with reproducible bleaching/coloring over 20 CA cycles (Figure S16). Nevertheless, the $-CE_{in}$ and CE_{out} values calculated were lower than those reported in the literature for analogous systems (Table 1).[10a,11,13a] The ECD@Er[Bmim]Cl device was then stored and kept in rest for ca. 3 years. To reproduce as much as possible real conditions, the device was not maintained in a glove box under controlled temperature, humidity and atmosphere, but was placed instead in a closed Petri dish in a dark location. After this period of time, both ECDs were subjected to the following steps: (1) 6 CV cycles (±2.0 V, 30 mV s^{-1}); (2) 6 CV cycles (±2.5 V, 30 mV s^{-1}); (3) 6 CV cycles (±3.0 V, 30 mV s^{-1}); and (4) 50 CA cycles (±2.5 V, at every 50 s). The T values were then obtained for +2.0/−2.0 V, +2.5/−2.5 V and +3.0/−3.0 V at 555 and 1200 nm. Figures 4a and 4b and Table S2 demonstrate that the T values progressively decreased upon application of the above voltages, and that the corresponding optical contrast (ΔT) values increased concomitantly at 555/1200 nm: 4.14/6.85%, 10.24/13.91% and 12.08/16.31% for ECD@Er[Bmim]Cl, and 3.93/3.99%, 4.44/4.57% and 5.75/5.12% for ECD@Er (Table 1). Higher ΔT values were found for the ECD@Er[Bmim]Cl device than for the ECD devoid of IL (ECD@Er). Accordingly, optical density (ΔOD) values were also found to be higher for the device incorporating [Bmim]Cl. It should be highlighted that some of these values were even better than some reported in Table 1 for analogous devices. Regarding the CE values, ECD@Er[Bmim]Cl also led to higher $-CE_{in}$ and CE_{out} values than ECD@Er both at 555 and 1200 nm (Table 1).

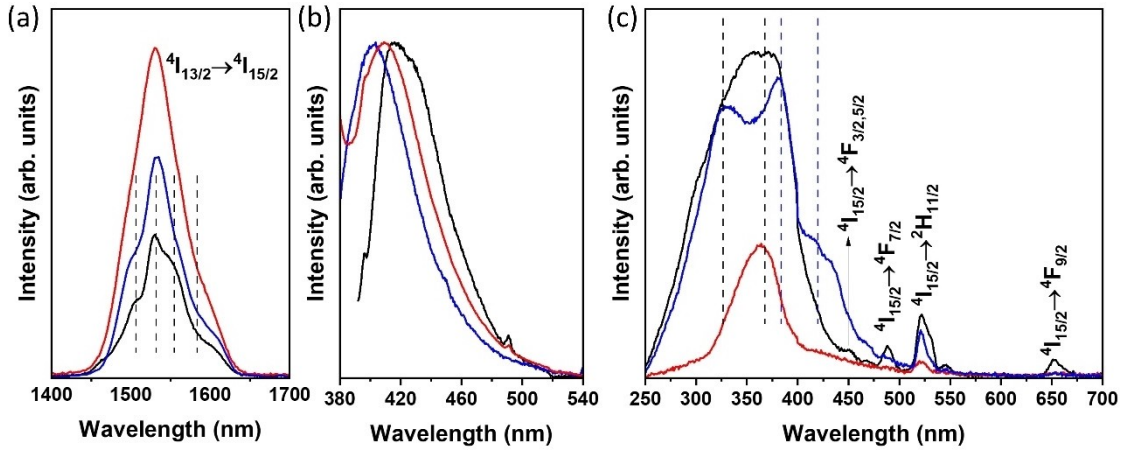

Figure 3. Emission spectra in the (a) NIR and (b) visible spectral region excited at 365 nm, and (c) Excitation spectra monitored at 1530 nm for $Er(tta)_3(H_2O)_2$ (black line), d-Ut$(600)_{400}Er(tta)_3(H_2O)_2$ (red line) and d-Ut$(600)_{400}Er(tta)_3(H_2O)_2$[Bmim]Cl (blue line).

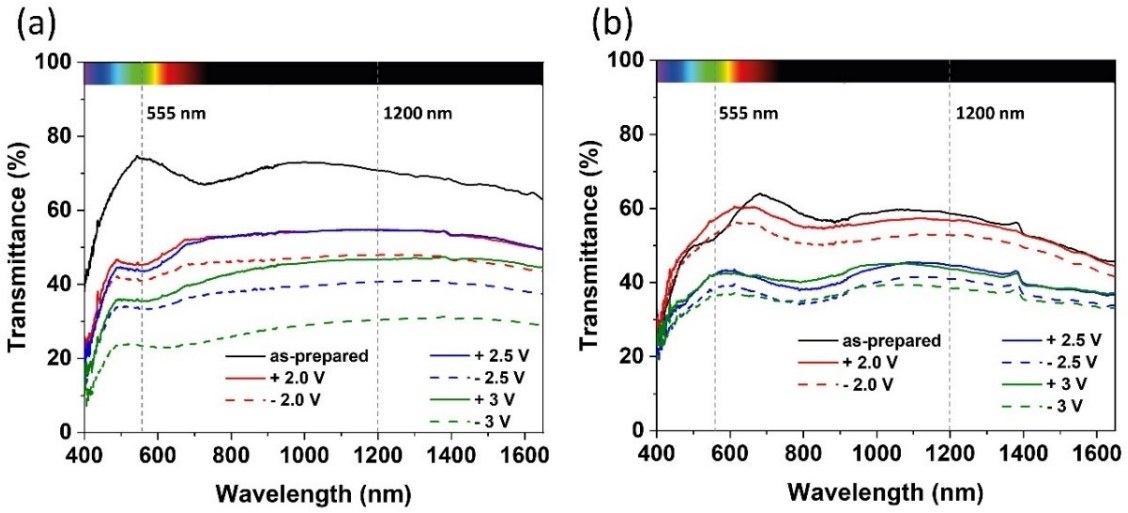

Figure 4. Visible-NIR spectra of the (a) ECD@Er[Bmim]Cl and (b) ECD@Er prototype devices: bleached (solid lines) and colored (dotted lines) states. Values measured during CV cycling measurements.

Interestingly, ECD@Er[Bmim]Cl denoted a self-improvement upon cycling (CE_{in}/CE_{out} in region $V > CE_{in}/CE_{out}$ in region I, Table 1).

Comparison of the performance of ECD@Er[Bmim]Cl back in 2019 and currently leads us to immediately conclude that the ECD underwent an amazing recovery leading to outstanding CE values, exhibiting two orders of magnitude higher than those measured 3 years ago (Table 1 and Figure 5). From these results we may also infer that the storage of the ECD@Er[Bmim]Cl ECD for a long period of time, in the dark and at room temperature, was beneficial, as it forced the device to return to its original state, and even improve its performance. This sort of observation is not, however, unprecedented. One of the most critical issues that affects the electrochemical devices whose operation relies on prolonged cycling, *i.e.*, ion insertion/extraction (*e.g.*, ECDs and batteries) is the long-term loss of performance. Sustainable galvanostatic and potentiostatic rejuvenation procedures were proposed in the literature for ECD devices, leading

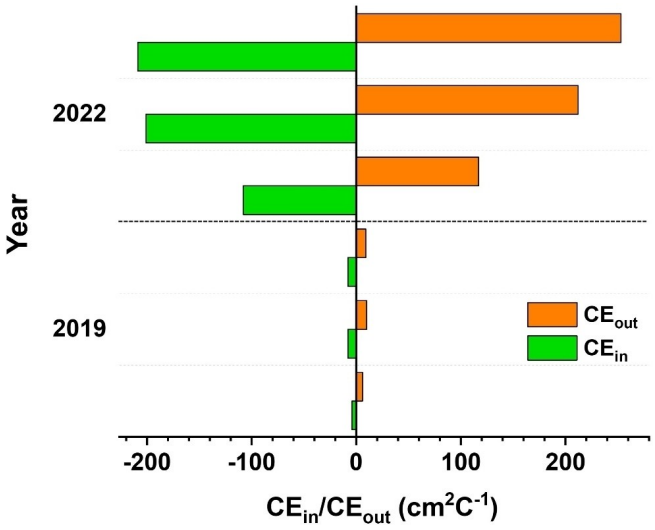

Figure 5. Performance improvement at 555 nm after 3-year device storage.

Table 1. Electro-optical performance of the ECD@Er[Bmim]Cl and ECD@Er prototype devices.

Hybrid Host	Doping Agent	TCO[a]	$T_{as\text{-}prepared}$ [%]		Test Date	Applied Voltage [V]	ΔT^{d} [%]		ΔOD		CA Interval[e]	CE_{in} [cm^2C^{-1}]	CE_{out} [cm^2C^{-1}]	CE_{in} [cm^2C^{-1}]	CE_{out} [cm^2C^{-1}]	Ref.
			λ [nm]				λ [nm]		λ [nm]			[nm]				
			555	1200			555	1200	555	1200		555	555	1200	1200	
d-Ut(600)	$Er(tta)_3(H_2O)_2$[Bmim]Cl	a-IZO	74	71	07/2019	±2.0	10.32	–	0.07	–	I	−4	6	–	–	This work
											II	−8	10	–	–	
											III	−8	9	–	–	
					11/2022	±2.0	4.14	6.85	0.04	0.06		–	–	–	–	
						±2.5	10.24	13.91	0.12	0.13	I	−108	117	−136	148	
											II	−201	212	−211	222	
											III	−209	253	−216	262	
											IV	−234	243	−247	256	
											V	−302	309	−300	307	
						±3.0	12.08	16.31	0.18	0.19		–	–	–	–	
	$Er(tta)_3(H_2O)_2$		51	59	11/2022	±2.0	3.93	3.99	0.03	0.03		–	–	–	–	This work
						±2.5	4.44	4.57	0.05	0.05	I	−43	60	−42	59	
											II	−38	46	−66	80	
											III	−134	114	−129	109	
											IV	−57	62	−50	54	
											V	−67	68	−62	64	
						±3.0	5.75	5.12	0.06	0.05		–	–	–	–	
d-U(600)	$LiBF_4$[Bmim]Cl		78	–	–	±2.0	7.9	–	0.05	–		–	–	–	–	[13a]
						±2.5	14.6	–	0.12	–		–	–	–	–	
						±3.0	16.5	–	0.13	–	I	−88	26	–	–	
											II	−111	44	–	–	
											III	−421	111	–	–	
d-Ut(600)	$LiCF_3SO_3$[BmimCl]	ITO[b]	73	–	–	−1.0	17	–	0.11	–		−6727	2794	–	–	[10a]
						−1.5	39	–	0.31	–		–	–	–	–	
						−2.0	66	–	0.83	–		–	–	–	–	
						−2.5	70		1.06	–		–	–	–	–	
d-PCL(530)	$LiCF_3SO_3.Er(tta)_3(H_2O)_2$	IMO[c]	64	–	–	±3.5	–	–	–	–		−8243	5200	–	–	[11]
						±4.0	8.9	–	0.07	–		–	–	–	–	

[a] Transparent conductive oxide layer; [b] Tin-doped indium oxide; [c] Molybdenum-doped indium oxide; [d] 3th CV cycle; [e] CA interval analyzed, please see Figure S16 (2019) and Figure S17 (2022).

Chemistry Europe
European Chemical Societies Publishing

to a very significant restauration of charge capacity.[28] The degradation process was found to be associated with the irreversible ion incorporation in the cathodically coloring EC layer (ion trapping), whereas the rejuvenation process was related to current- and voltage-induced removal of the same ions (detrapping/bleaching). But mass transport of the ions through the electrolyte may also be responsible for performance drop. For instance, the electrolyte decomposition and the corresponding formation of solid electrolyte interface (SEI) is the main aging process in most graphite-based lithium-ion batteries, leading to an irreversible capacity loss (due to loss of active lithium) and impedance increase (due to the increase in film layer thickness).[29] It is known that keeping a battery in a fully discharged state at rest is a potential source for prolonging battery life as long as the battery behavior is stable with temperature. Long rest periods can help a battery maintain longer the so-called polarization recovery stages, which allow the species to spread more evenly, therefore increasing the battery capacity.[30] Thus, the performance recovery reported in the present work is not surprising, since the working principle of an ECD is *grosso modo* that of a battery.

The operation of the ECD@Er[Bmim]Cl and ECD@Er devices over 50 CA cycles (±2.5 V at every 50 s) was examined and the transmittance values were measured at 555 and 1200 nm (Figure 6 and Table S3). Figures 6a and 6b allow inferring that both devices displayed excellent cycling stability, and fast coloring kinetics. Figures 6c and 6d demonstrate their excellent optical modulation stability. As mentioned above, the performance of ECD@Er[Bmim]Cl is definitely superior, with considerably higher $-CE_{in}$ and CE_{out} values (Table 1). The response times for ECD@Er[Bmim]Cl were 30–40 s for coloring and 1.2 min for bleaching (see Video), indicating that the coloring kinetics are faster than the bleaching kinetics.

Optical memory tests were performed over 60 days. Figure 7a demonstrates that the ECD@Er[Bmim]Cl presented exceptionally good performance since a loss of the T value of only 15–18% occurred after remaining this long period of time under open circuit. In the case of the ECD@Er the loss of T value reached 20–26% (Figure 7b).

It is of interest to compare at this stage the best results found in this work with those reported in literature for analogous ECDs.

In the case of an ECD incorporating also a-IZO as TCOs, but incorporating the di-ureasil electrolyte d-U(600)$LiBF_4$[Bmim]Cl (where $LiBF_4$ is lithium tetrafluoroborate),[13a] instead of d-Ut(600)$_{400}$Er(tta)$_3$(H_2O)$_2$[Bmim]Cl, the ΔT, ΔOD and CE values are similar (Table 1). We note that the ionic conductivity of d-Ut(600)$_{400}$Er(tta)$_3$(H_2O)$_2$[Bmim]Cl (4.68×10^{-5} S cm^{-1}) and d-U-

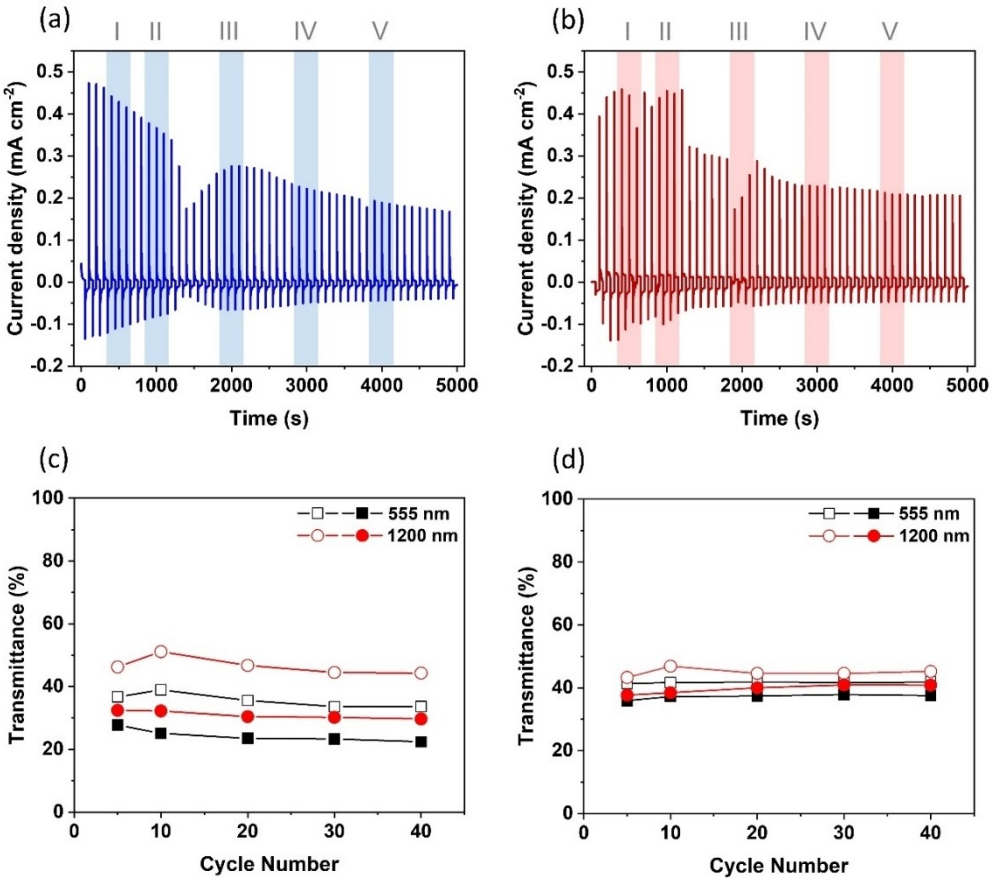

Figure 6. Cycling performance of the ECD@Er[Bmim]Cl (a,c) and ECD@Er (b, d) devices over 50 cycles (±2.5 V at every 50 s). Current density over time (a, b) and transmittance at 555 and 1200 nm over cycle number (c, d) (bleached state, open symbols, and colored state, closed symbols). The vertical colored bars indicate the time intervals for which the CE values were calculated. Figure S17 shows in detail these intervals.

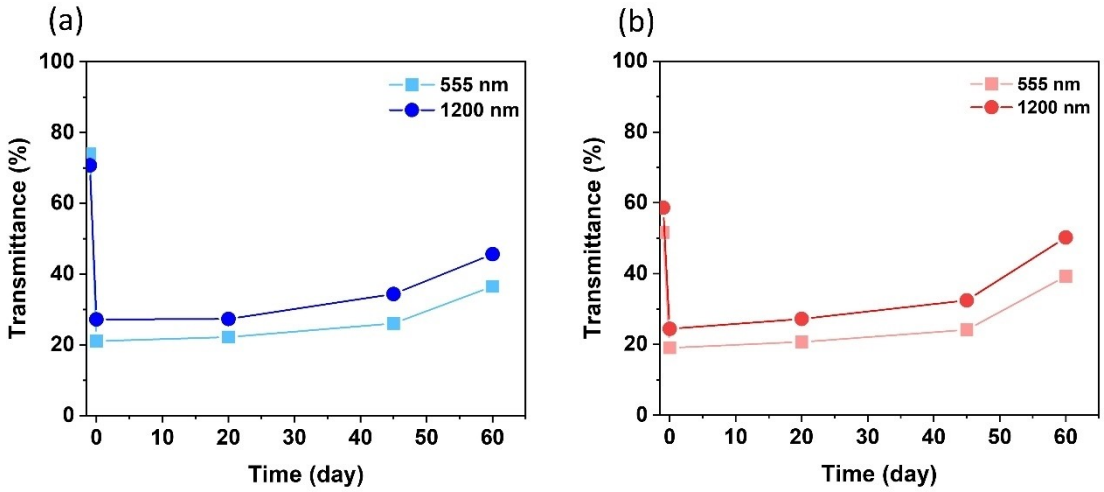

Figure 7. Optical-circuit memory test of the ECD@Er[Bmim]Cl (a) and ECD@Er (b) devices.

(600)$LiBF_4$[Bmim]Cl (8.10×10^{-5} S cm^{-1})[13a] do not differ significantly at room temperature.

In contrast, ECDs with different TCO layers and incorporating di-urethanesil electrolytes doped with lithium triflate ($LiCF_3SO_3$) and [Bmim]Cl[10a,11] (Table 1) or a mixture of $LiCF_3SO_3$ and $Er(tta)_3(H_2O)_2$[10a,11] (Table 1) presented significantly higher CE values than ECD@Er[Bmim]Cl. We must note, however, that d-Ut(600)$_{400}$Er(tta)$_3$(H$_2$O)$_2$[Bmim]Cl exhibits higher room temperature ionic conductivity than d-Ut(600)$LiCF_3SO_3$[BmimCl] and d-PCL(530)$LiCF_3SO_3$.Er(tta)$_3$(H$_2$O)$_2$ (3.64×10^{-6} S cm^{-1},[10a] and 3.68×10^{-6} S cm^{-1},[11] respectively).

For the sake of clarity, the hypothetical dual-mode operation of the ECD@Er[Bmim]Cl and ECD@Er devices is provided in Figures 8a and 8c, together with the quantification of the coloration (Figure 8b). The as-prepared devices displayed T values of *ca.* 74/51% and 71/59% at 555/1200 nm, respectively (Figure 4) and light-yellow (L* = 84.39, a* = −4.17 and b* = 10.78) and yellow-green (L* = 80.88, a* = −3.55 and b* = 15.07) color hues (Figures 8a and 8b and Table S4). At the end of 6 CV cycles (± 2.5 V, 30 mV s^{-1}) ECD@Er[Bmim]Cl and ECD@Er exhibited a dark blue and light blue color, respectively (Figures 8a and 8b and Table S4), pushing the T values down to *ca.* 44/42% and 55/45% at 555/1200 nm, respectively (Table S2 and Figures 8c and 8d).

There are several requirements for the ideal window:[31] (1) If the building is located in a cold climate region, the window should allow visible and NIR radiation to enter, reflect UV radiation from outdoors, and reflect all radiation from indoors. (2) If the building is located in a hot climate region, the window should allow visible light to enter, reflect NIR and UV radiations, and be completely transparent to the NIR radiation from indoors. Values of T > 70% and 60% for the visible solar transmittance for both types of windows were proposed by Piccolo and Simone,[32] respectively. Considering the attributes of ECD@Er[Bmim]Cl, which offers bright hot and semi-bright warm modes, we are led to suggest that it would be a good solution for a window of a building located in a cold climate region. However, the levels of solar transmittance attained in the bleached and colored states (33.45/40.75% and 43.69/54.66% at 555/1200 nm, respectively) thus lower than the sought ones, lead us to suggest that, while their deployment in window façades would not be suitable, they would be applicable in other areas of a building where obstructed view is irrelevant (skylights, roof lights, upper windows, inclined glazing, privacy glazing, and façade elements). The fact that this ECD is able to convert UV/visible to heat transforms this window into a heat generator system.

Conclusions

Herein, a novel di-urethane cross-linked POE/siloxane hybrid system (di-urethanesil (dUt(600)) doped solely with the Er(tta)$_3$(H$_2$O)$_2$ complex and a mixture of Er(tta)$_3$(H$_2$O)$_2$ and [Bmim]Cl was synthetized, aiming at the development of highly NIR luminescent hybrids for applications in environmentally friendly ECDs able to control the solar visible and NIR radiation and generate heat.

The structure, topography, surface free energy, ionic conductivity, and optical features of the two electrolytes were characterized. The d-Ut(600)$_{400}$Er(tta)$_3$(H$_2$O)$_2$[Bmim]Cl electrolyte was produced as a homogenous, transparent, slightly rough film, with higher ionic conductivity than d-Ut(600)$_{400}$Er(tta)$_3$(H$_2$O)$_2$. Photoluminescence studies confirmed that both electrolyte films presented a typical Er^{3+} NIR emission around 1550 nm and also a broad band in the UV/blue spectral region. The ECD@Er[Bmim]Cl prototype device, which was kept in rest for ca. 3 years, demonstrated an amazing recovery, revealing fast switching time, high optical and coloration efficiency, and excellent cycling stability and memory effect.

This heat generation device offers a bright hot and a semi-bright warm modulation operation suitable for buildings located in a cold climate region. The technical performance of such smart windows is appropriate for particular areas of the building, such as skylights, roof lights, upper windows, inclined glazing, and privacy glazing.

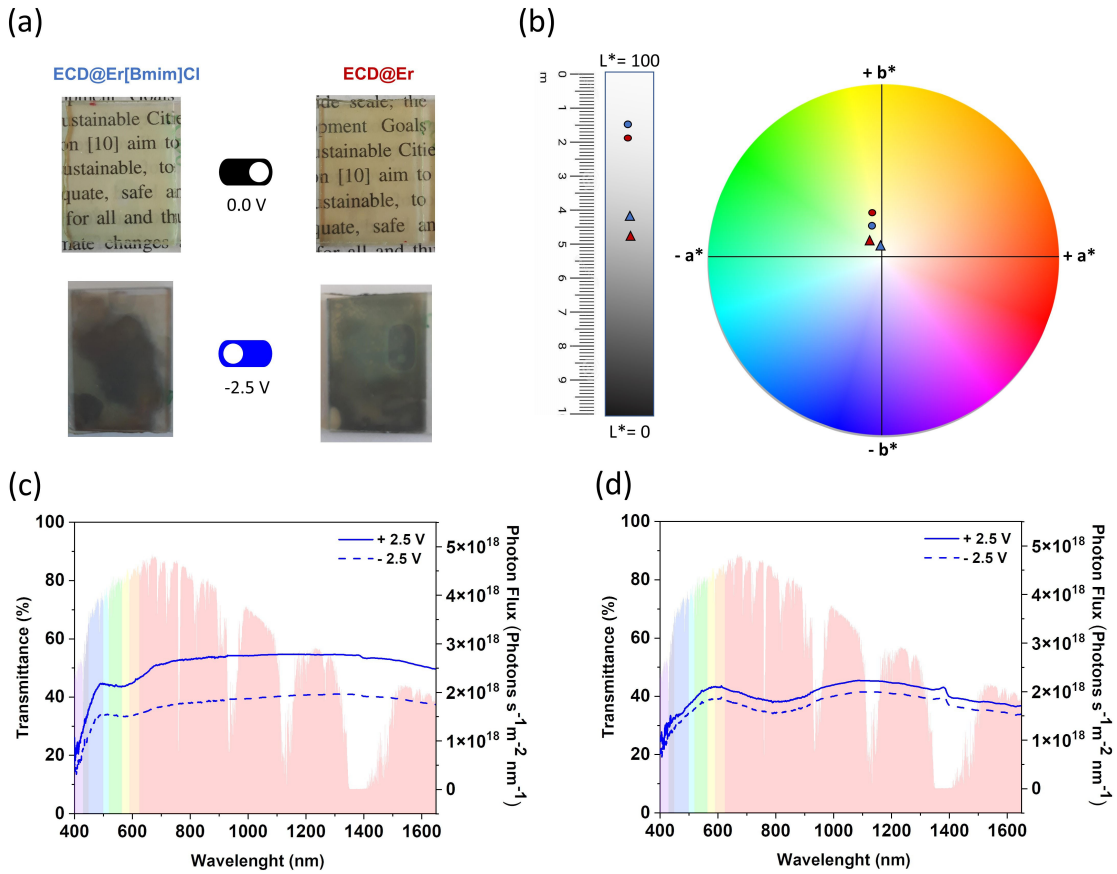

Figure 8. Ideal dual-mode operation of the ECD@Er[Bmim]Cl (blue color) and ECD@Er (red color) devices: (**a**) as-prepared and colored state at −2.5 V and (**b**) 1976 CIE L*a*b* color coordinates. The circles correspond to the as-prepared values and the triangles correspond to the values measured after applying a voltage of −2.5 V. Visible-NIR spectra of the (**c**) ECD@Er[Bmim]Cl and (**d**) ECD@Er prototype devices: bright hot (bleached, solid lines) and semi-bright warm (colored, dotted lines) states (±2.5 V). The shadowed area represents the AM1.5 G solar spectral irradiance spectrum.[33]

In terms of NIR emission, our findings suggest that ECD@Er would be, however, a better choice.

In conclusion, we present here a proof-of-concept of an ECD able to convert UV/visible radiation into heat with foreseen application in certain types of building windows. This work highlights the critical role played by the electrolyte (host matrix and doping agents) and TCO nature on the electro-optical performance of ECD devices. Future developments of the present ECD concept will address the assembly and testing of large-area ECD devices.

Experimental Section

Materials

Thenoyltrifluoracetone (Htta, 99%, Sigma-Aldrich), 3-isocyanatepropyltriethoxysilane (ICPTES, 95%, Across Organics), erbium(III) chloride hexahydrate ($ErCl_3.6H_2O$, 99%, Sigma-Aldrich), 1-butyl-3-methylimidazolium chloride ([Bmim]Cl, 98%, Thermo Scientific), sodium hydroxide (NaOH, Merck), ethanol (EtOH, 99.8%, Fluka) and diiodomethane (99%, stab. CH_2I_2, Thermo Scientific) were used without further purification. Poly(ethylene glycol) (PEG(600), molecular weight ≈600 g mol^{-1}, Sigma-Aldrich) and tetrahydrofuran (THF, Fisher Scientific) were kept over molecular sieves. All the experiments were performed with ultra-pure water at pH = 5.4 (Interlab).

Synthesis

Synthesis of $Er(tta)_3(H_2O)_2$

Bisaquatris(thenoyltrifluoroacetonate) erbium (III) ($Er(tta)_3(H_2O)_2$) was prepared using the conventional method described elsewhere.[11] For further information, please see the synthesis section in the SI.

Synthesis of the d-Ut(600)$_{400}$Er(tta)$_3$(H$_2$O)$_2$ and d-Ut(600)$_{400}$Er(tta)$_3$(H$_2$O)$_2$[Bmim]Cl di-urethanesils

The doped sol-gel derived di-urethanesils described in the present work were prepared through a previously reported methodology.[34] For more details, please see the synthesis section in the SI and Figure S18.

Characterization

ATR/FT-IR spectra (4000–400 cm^{-1}) were registered at room temperature with a IRAffinity-1S Shimadzu FT-IR spectrometer (ATR accessory with a diamond crystal), from Thermo Scientific. The apparatus was operated with the Omnic software from Thermo

Fisher Scientific. Samples were performed with 180 scans at a resolution of 4 cm^{-1}. Band deconvolution was performed using the iterative least-squares curve-fitting method with PeakFit software.[35] Through the variation of the width, frequency and intensity of the bands, the best fit was achieved. Curve-fitting was performed by means of a Voigt function using a linear baseline correction with a tolerance of 0.2%. The standard errors of the curve-fitting process were lower than 0.002.

Static CA measurements, using the sessile drop technique, were performed to evaluate the wettability of the d-Ut$(600)_{400}$Er-$(tta)_3(H_2O)_2$ and d-Ut$(600)_{400}$Er$(tta)_3(H_2O)_2$[Bmim]Cl electrolytes (Figure S19). In a temperature-controlled chamber at 25 ± 1 °C, CA were obtained by means of a Krüss DSA25S drop shape analyzer controlled by the software ADVANCE. Liquid droplets of 5 μL were used in all tests. Via the Young-Laplace fitting, CA were calculated from digital images obtained by a video camera. The CA values were obtained from four different spots. In each spot ten measurements were performed. The reported values are the average of all the measurements. Data error analysis were obtained through the arithmetic mean of the root mean square error.

To calculate the SFE of the solid surfaces of d-Ut$(600)_{400}$Er-$(tta)_3(H_2O)_2$ and d-Ut$(600)_{400}$Er$(tta)_3(H_2O)_2$[Bmim]Cl, as well as its dispersive and polar components, we used the Owens, Wendt, Rabel, and Kaelble (OWRK) method (Eq. 1):[36]

$$\gamma_{LV}(1+\cos\theta) = 2\left(\sqrt{\gamma_{LV}^{d}\,\gamma_{SV}^{d}} + \sqrt{\gamma_{LV}^{p}\,\gamma_{SV}^{p}}\right) \quad (1)$$

where γ_{LV}, is the surface tension between the liquid and vapor (air), γ_{LV}^{d} and γ_{LV}^{p} are its dispersive (*e.g.*, London dispersion forces), and polar (*e.g.* hydrogen bonding) components and γ_{SV}^{d} and γ_{SV}^{p} are the dispersive and polar components of γ_{SV} (*i.e.*, SFE). Eq. 1 allows calculating γ_{SV}^{d}, γ_{SV}^{p} and SFE. The method requires CA measurements with at least two test liquids with γ_{LV}^{d} and γ_{LV}^{p} values reported in the literature. One of these liquids must be predominantly polar and the second liquid must be dispersive. Usually the chosen liquids are water and diiodomethane, respectively. It should be noted that the OWRK model implies the use of a high purity liquid, a smooth and chemically homogenous solid, and the absence of chemical reactions between the liquid and the solid. The OWRK model is a powerful model that has found widespread acceptation both in research and industry contexts. The relationship between SFE, γ_{LV}, and CA may be visualized using the so-called wetting envelope plots. These are based on the OWRK equation, rewritten in terms of polar coordinates. The wetting envelopes of the two electrolytes studied were built using the Excel spreadsheet provided by Nanoscience.[37]

AFM images were obtained with a Nano-Observer AFM microscope (CSIntruments AFM Microscopes-France) in tapping mode, using a spring constant of 0.3 $N\,m^{-1}$ and a super sharp Si HQ:NSC19/FORTA probe with a frequency resonance of 60 kHz. Gwyddion 2.61 software was used for data visualization and analysis.

Ionic conductivity values were obtained by the complex plane impedance technique using an Autolab PGSTAT-12 (Eco Chemie) equipment, at frequencies between 65 kHz and 0.5 Hz and in a temperature range from 23 to 104 °C (Buchi TO51 tube oven with a K thermocouple). During the measurements, the ormolytes were placed between 10 mm diameter gold electrodes (Goodfellow, > 99.9%).

SEM and EDX spectroscopy analyses were performed with a FEI Quanta 650 FEG microscope under high vacuum at the Iberian Nanotechnology Laboratory. Secondary electrons were detected by an Everhardt Thornley SED (secondary electron detector); for element analysis an EDX detector (Oxford Instruments) was used. The images were acquired at 15 kV and spot size 3. The samples were sputtered with gold, using the Leica EM ACE200 and using the following setup: sputtering current = 30 mA and duration = 60 s.

The photoluminescence and time-resolved photoluminescence data were acquired under ambient conditions with a FluoTime 300 spectrometer from PicoQuant (Berlin, Germany). A 450 W Xe arc lamp excitation source, and two detectors, one for the visible spectral region (Low dark current hybrid photomultiplier, PicoQuant, Model PMA 192) and one for the NIR (Hamamatsu, Model H10330C-75) spectral region were used. Corrections of the emission spectra, for detection and optical spectral response of the spectrofluorimeter, and of the excitation spectra, for the spectral distribution of the lamp intensity using a photodiode reference detector, were made. The room temperature emission quantum yield values were obtained using a Hamamatsu C9920-02 system with a 150 W xenon lamp coupled to a monochromator for wavelength discrimination, an integrating sphere as the sample chamber, and a multichannel analyzer for signal detection. The method is accurate to within 10%. The optical parameters of the transmitted light were registered by means of an integrating sphere (ISP 150 L, Instrument Systems) connected to a detector (MAS40-121, Instrument Systems), with an integration time of 10 s.

Assembly of the ECDs prototypes

Two 5-layer ECDs were tested (Figure 1): glass/a-IZO/c-NiO/d-Ut-$(600)_{400}$Er$(tta)_3(H_2O)_2$)/a-WO_3/a-IZO/glass and glass/a-IZO/c-NiO/d-Ut$(600)_{400}$Er$(tta)_3(H_2O)_2$[Bmim]Cl)/a-WO_3/a-IZO/glass. The notations ECD@Er and ECD@Er[Bmim]Cl were used to represent them, respectively.

The outermost ECD layers – a-IZO thin films – were deposited by sputtering on glass plates, using a homemade system (from In_2O_3/ZnO 89.3/10.7 wt%, 99.99%, 3 mm diameter×6 mm thick, Super Conductive Materials). The sputtering was performed at room temperature and at a deposition pressure (argon and oxygen) constant value of 0.13 Pa. The distance between the target and the substrate was 10 cm, and the radio frequency power was 100 W.

Sputtering and e-beam evaporation were used to deposit the EC layers of the ECDs, *i.e.*, a-WO_3 and c-NiO, on a-IZO-coated glass plates, respectively. A 300 nm-thick a-WO_3 layer was deposited using a Pfeiffer Vacuum Classic 500 system with a 3" diameter ceramic target (Plasmaterials), at an oxygen atmosphere (oxygen partial pressure of 0.2 Pa) and argon environment using a deposition pressure of 1.0 Pa, and a radio frequency power of 200 W. A 300 nm-thick polycrystalline c-NiO thin layer was deposited, from NiO commercial pellets random pieces (3–6 mm, 99.99%, Super Conductive Materials), by e-beam evaporation in a homemade system, with a primary chamber pressure of 7×10^{-4} Pa and evolution rate of 6 $nm\,min^{-1}$.

ECD@Er and ECD@Er[Bmim]Cl prototypes with an active area of 1.8 cm×2.5 cm were assembled in the open air. A small volume of the d-Ut$(600)_{400}$Er$(tta)_3(H_2O)_2$ and d-Ut$(600)_{400}$Er$(tta)_3(H_2O)_2$[Bmim]Cl sols was cast onto the surface of a-WO_3/a-IZO and c-NiO/a-IZO glass plates, respectively (Figure 1a). After solvent evaporation, the c-NiO/a-IZO glass plate was positioned over the top of the a-WO_3/a-IZO glass plate to sandwich the electrolyte between the two EC layers. To ensure the electrical contacts, free area was left in one end of each of the glass plates. The assembled system was then pressed together and kept in rest until the electro-optical analyses (Figure 1b).

Characterization of the ECDs

The T of the ECDs was registered in the 400–1650 nm spectral range using a DH Mini, UV-Vis-NIR Lightsource Ocean Optics and a halogen lamp. The CV and CA analyses were performed using a Gamry potentiostat/galvanostat/ZRA 11107, taking the c-NiO/a-IZO layer as the counter and reference electrodes, and the a-WO_3/a-IZO layer as the working electrode. The inserted and disinserted charge density (Q_{in} and Q_{out}, respectively) values were calculated by integrating the CA curves during coloring and bleaching, respectively, at certain cycles.

The evaluation of the electro-optical performance of the ECDs implied the calculation of several parameters: switching speed (response time for coloring/bleaching), optical contrast (transmittance change $\Delta T = T_{bleached} - T_{colored}$, in %, at a specified wavelength or range of wavelengths), optical density ($\Delta OD = -\log(T_{colored}/T_{bleached})$), coloration efficiency ($CE = \Delta OD/\Delta Q$) and cycling stability. To deduce the CE values, the cathodic and anodic charge densities (Q_{in} and Q_{out}, respectively) were calculated by integrating the CA curves during the coloring and bleaching processes, respectively, for a given cycle and for a given wavenumber.

The 1976 Commission Internationale d'Éclairage (CIE) L*a*b* color coordinates (L* is the lightness (0 = black, 100 = white), a* is a red-green balance (+a* = red and −a* = green), and b* is a yellow-blue balance (+b* = yellow and −b* = blue)) of the bleached and colored states of the ECDs were calculated using a Chroma Meter CR-300 Minolta (Osaka, Japan). The values indicated represent the average of three independent measurements performed in different locations of each prototype, with the standard deviation being less than 2%.

Supporting Information

[1] V. de Zea Bermudez, D. Ostrovskii, M. C. Gonçalves, L. D. Carlos, R. A. S. Ferreira, L. Reis, P. Jacobsson, *Phys. Chem. Chem. Phys.* **2004**, *6*, 638.

[2] Y. Gao, R. Guo, R. Fan, Z. Liu, W. Kong, P. Zhang, F.-p. Du, *Pest Manag. Sci.* **2018**, *74*, 1804.

[3] F. Kafiah, T. Laoui, E. Abdelsalam, M. A. Atieh, Z. Khan, M. Alkasrawi, *Membranes* **2020**, *10*, 0358.

Supplementary Materials

Supplementary material can be found, in the online version, at https://doi.org/10.1002/celc.202300479.

Video showing the bleaching/coloring operation of ECD@Er-[Bmim]Cl (MP4)

Author Contributions

Daniela Pinheiro: Conceptualization, Methodology, Validation, Formal analysis, Investigation, Writing – Original Draft, Writing – Review & Editing, Visualization. *Mariana Fernandes:* Formal analysis, Investigation, Validation. *Rui F. P. Pereira:* Formal analysis, Investigation, Writing – Original Draft. *Sónia Pereira:* Resources, Investigation. *Sandra F. Correia:* Formal analysis, Investigation. *M. Manuela Silva:* Validation. *Elvira Fortunato:* Resources, Validation. *Rute A. S. Ferreira:* Validation, Writing – Review & Editing. *Maria Cristina Gonçalves:* Conceptualization, Validation, Writing – Review & Editing, Supervision. *Verónica de Zea Bermudez:* Conceptualization, Validation, Writing – Review & Editing, Visualization, Supervision, Project administration, Funding acquisition.

Acknowledgements

This work was funded by project I&D&I OBTAIN, (NORTE-01-0145-FEDER-000084), co-financed by the FEDER through NORTE 2020, CENTRO2020 in the scope of the project PLANET, (CENTRO-01-0247-FEDER-181242), project SOLPOWINS (PTDC/CTM/4304/2020), CQ-VR that is supported by FCT (UIDB/00616/2020 and UIDP/00616/2020) and CICECO-Aveiro Institute of Materials (UIDB/50011/2020, UIDP/50011/2020 & LA/P/0006/2020), financed by national funds through the FCT/MCTES (PIDDAC). D. Pinheiro acknowledges OBTAIN for post-doc grant BIPD/UTAD/19/2021. R. Pereira and M. Fernandes acknowledge FCTU-Minho and FCT-UTAD, respectively, for the contracts in the scope of Decreto-Lei 57/2016 57/2017. S. Correia thanks FCT for the researcher contract (2022.03740.CEECIND).

Conflict of Interests

The authors declare no conflict of interest.

Data Availability Statement

Data will be made available on request.

Keywords: electrochromic windows · erbium complex · NIR emitting electrolytes · visible/NIR transparent conducting oxides · zero-energy buildings

[1] *Regulation (EU) 2021/1119 of the European Parliament and of the Council of 30 June 2021 establishing the framework for achieving climate neutrality and amending Regulations (EC) No 401/2009 and (EU) 2018/1999 ('European Climate Law')*, **2021**.

[2] a) J. Liu, R. Yang, J. Zhang, Q. Tao, A. Li, Z. Liu, Y. Su, Y. Liu, *Sol. Energy Mater. Sol. Cells* **2023**, *249*, 112048; b) A. Ahmed, T. Ge, J. Peng, W.-C. Yan, B. T. Tee, S. You, *Energy Build.* **2022**, *256*, 111755; c) M. W. Akram, M. F. Mohd Zublie, M. Hasanuzzaman, N. A. Rahim, *Sustainability* **2022**, *14*, 1316; d) A. Cannavale, U. Ayr, F. Fiorito, F. Martellotta, *Energies* **2020**, *13*, 1449.

[3] http://www.un.org/sustainabledevelopment/, **accessed March 2023**.

[4] https://ec.europa.eu/info/funding-tenders/opportunities/docs/2021-2027/horizon/wp-call/2023-2024/wp-8-climate-energy-and-mobility_horizon-2023-2024_en.pdf, **accessed March 2023**.

[5] a) S. Zhao, B. Wang, N. Zhu, Y. Huang, F. Wang, R. Li, Y. Zhao, Q. Jiang, X. Wu, R. Zhang, *Carbon Neutralization* **2022**, *2*, 4; b) G. Syrrokostas, G. Leftheriotis, S. N. Yannopoulos, *Renewable Sustainable Energy Rev.* **2022**, *162*, 112462; c) B. Yang, G. Yang, Y.-M. Zhang, S. X.-A. Zhang, *J. Mater. Chem. C* **2021**, *9*, 4730; d) R. Tällberg, B. P. Jelle, R. Loonen, T. Gao, M. Hamdy, *Sol. Energy Mater. Sol. Cells* **2019**, *200*, 109828; e) M. Casini, *Renewable Energy* **2018**, *119*, 923; f) N. C. Davy, M. Sezen-Edmonds, J. Gao, X. Lin, A. Liu, N. Yao, A. Kahn, Y.-L. Loo, *Nat. Energy* **2017**, *2*, 17104.

[6] a) C. Park, J. M. Kim, Y. Kim, S. Bae, M. Do, S. Im, S. Yoo, J. H. Kim, *ACS Appl. Electron. Mater.* **2021**, *3*, 4781; b) J. Kim, M. Rémond, D. Kim, H. Jang, E. Kim, *Adv. Mater. Technol.* **2020**, *5*, 1900890.
[7] a) Z. Kou, J. Wang, X. Tong, P. Lei, Y. Gao, S. Zhang, X. Cui, S. Wu, G. Cai, *Sol. Energy Mater. Sol. Cells.* **2023**, *254*, 112273; b) H. Liu, Y. Zhang, P. Lei, J. Feng, S. Jia, J. Huang, C. Hu, C. Bian, G. Cai, *ACS Appl. Mater. Interfaces* **2023**, *15*, 23412; c) R. Ren, S. Liu, Y. Gao, P. Lei, J. Wang, X. Tong, P. Zhang, Z. Wang, G. Cai, *ACS Energy Lett.* **2023**, *8*, 2300; d) X. Tong, J. Wang, P. Zhang, P. Lei, Y. Gao, R. Ren, S. Zhang, R. Zhu, G. Cai, *Chem. Eng. J.* **2023**, *470*, 144130; e) M. Barawi, G. Veramonti, M. Epifani, R. Giannuzzi, T. Sibillano, C. Giannini, A. Rougier, M. Manca, *J. Mater. Chem. A* **2018**, *6*, 10201; f) S. Zhang, S. Cao, T. Zhang, A. Fisher, J. Y. Lee, *Energy Environ. Sci.* **2018**, *11*, 2884; g) J. Xu, Y. Zhang, T.-T. Zhai, Z. Kuang, J. Li, Y. Wang, Z. Gao, Y.-Y. Song, X.-H. Xia, *ACS Nano* **2018**, *12*, 6895; h) A. Llordés, G. Garcia, J. Gazquez, D. J. Milliron, *Nature* **2013**, *500*, 323.
[8] a) K. Madasamy, D. Velayutham, V. Suryanarayanan, M. Kathiresan, K.-C. Ho, *J. Mater. Chem. C* **2019**, *7*, 4622; b) K. W. Shah, S.-X. Wang, D. X. Y. Soo, J. Xu, *Polymer* **2019**, *11*, 1839; c) S. Zhao, W. Huang, Z. Guan, B. Jin, D. Xiao, *Electrochim. Acta* **2019**, *298*, 533.
[9] P. Barquinha, G. Gonçalves, L. Pereira, R. Martins, E. Fortunato, *Thin Solid Films* **2007**, *515*, 8450.
[10] a) M. C. Gonçalves, R. F. P. Pereira, R. Alves, S. C. Nunes, M. Fernandes, H. M. R. Gonçalves, S. Pereira, M. M. Silva, E. Fortunato, R. Rego, V. de Zea Bermudez, *Front. Mater.* **2020**, *7*; b) M. C. Gonçalves, N. J. O. Silva, V. de Zea Bermudez, R. A. S. Ferreira, L. D. Carlos, K. Dahmouche, C. V. Santilli, D. Ostrovskii, I. C. Correia Vilela, A. F. Craievich, *J. Phys. Chem. B* **2005**, *109*, 20093; c) M. C. Gonçalves, V. de Zea Bermudez, R. A. S. Ferreira, L. D. Carlos, D. Ostrovskii, J. Rocha, *Chem. Mater.* **2004**, *16*, 2530.
[11] M. Fernandes, V. Freitas, S. Pereira, R. Leones, M. M. Silva, L. D. Carlos, E. Fortunato, R. A. S. Ferreira, R. Rego, V. de Zea Bermudez, *Energies* **2018**, *11*, 3513.
[12] a) M. Fernandes, V. de Zea Bermudez, in *Chemical Solution Synthesis for Materials Design and Thin Film Device Applications* (Eds: S. Das, S. Dhara), Elsevier **2021**, p. 439; b) S. Heusing, M. A. Aegerter, in *Sol-Gel Processing for Conventional and Alternative Energy*, DOI: 10.1007/978-1-4614-1957-0_12 (Eds: M. Aparicio, A. Jitianu, L. C. Klein), Springer US, Boston, MA **2012**, p. 239.
[13] a) P. J. Nunes, R. F. P. Pereira, S. Pereira, M. M. Silva, E. Fortunato, V. de Zea Bermudez, M. Fernandes, *Energies* **2023**, *16*, 426; b) S. C. Nunes, V. de Zea Bermudez, M. M. Silva, M. J. Smith, D. Ostrovskii, R. A. S. Ferreira, L. D. Carlos, J. Rocha, A. Gonçalves, E. Fortunato, *J. Mater. Chem.* **2007**, *17*, 4239.
[14] a) M. A. Cardoso, R. F. P. Pereira, S. Pereira, H. Gonçalves, M. M. Silva, L. D. Carlos, S. C. Nunes, E. Fortunato, R. A. S. Ferreira, R. Rego, V. de Zea Bermudez, *Adv. Sustainable Syst.* **2019**, *3*, 1800115; b) P. V. Rathod, J. M. C. Puguan, H. Kim, *Chem. Eng. J.* **2021**, *422*, 130065.
[15] a) H. M. R. Gonçalves, R. F. P. Pereira, E. Lepleux, L. Pacheco, A. J. M. Valente, A. J. Duarte, V. de Zea Bermudez, *Small* **2020**, *16*, 1907661; b) H. M. R. Gonçalves, R. F. P. Pereira, E. Lepleux, T. Carlier, L. Pacheco, S. Pereira, A. J. M. Valente, E. Fortunato, A. J. Duarte, V. de Zea Bermudez, *Adv. Sustainable Syst.* **2019**, *3*, 1900047; c) S. C. Nunes, R. F. P. Pereira, N. Sousa, M. M. Silva, P. Almeida, F. M. L. Figueiredo, V. de Zea Bermudez, *Adv. Sustainable Syst.* **2017**, *1*, 1700070.
[16] a) K. Fujita, R. Nakano, R. Nakaba, N. Nakamura, H. Ohno, *Chem. Commun.* **2019**, *55*, 3578; b) H. Hajfarajollah, B. Mokhtarani, A. sharifi, M. Mirzaei, A. Afaghi, *RSC Adv.* **2014**, *4*, 13153.
[17] a) A. Efimova, G. Hubrig, P. Schmidt, *Thermochim. Acta* **2013**, *573*, 162; b) O. Ryosuke, H. Satoshi, S. Satyen, K. Akiko, H. Hiro-o, *Chem. Lett.* **2003**, *32*, 948.
[18] a) J. D. Holbrey, W. M. Reichert, M. Nieuwenhuyzen, S. Johnson, K. R. Seddon, R. D. Rogers, *Chem. Commun.* **2003**, 1636–1637; b) H. Satoshi, O. Ryosuke, H. Hiro-o, *Chem. Lett.* **2003**, *32*, 498; c) S. Satyen, H. Satoshi, K. Akiko, H. Hiro-o, *Chem. Lett.* **2003**, *32*, 740; d) J. L. Anderson, J. Ding, T. Welton, D. W. Armstrong, *J. Am. Chem. Soc.* **2002**, *124*, 14247.
[19] J.-C. G. Bünzli, C. Piguet, *Chem. Soc. Rev.* **2005**, *34*, 1048.
[20] a) S. S. Nobre, R. A. S. Ferreira, X. Cattoën, S. Benyahya, M. Taillefer, V. de Zea Bermudez, M. W. Chi Man, L. D. Carlos, *Spectrosc. Lett.* **2010**, *43*, 321; b) L. D. Carlos, R. A. S. Ferreira, V. de Zea Bermudez, S. J. L. Ribeiro, *Adv. Mater.* **2009**, *21*, 509.
[21] S. C. Nunes, S. M. Saraiva, R. F. P. Pereira, S. Pereira, M. M. Silva, L. D. Carlos, E. Fortunato, R. A. S. Ferreira, R. Rego, V. d Zea Bermudez, *ACS Appl. Energ. Mater.* **2019**, *2*, 1951.
[22] M. Fernandes, V. de Zea Bermudez, R. A. S. Ferreira, L. D. Carlos, A. Charas, J. Morgado, M. M. Silva, M. J. Smith, *Chem. Mater.* **2007**, *19*, 3892.
[23] S. F. H. Correia, P. P. Lima, P. S. André, R. A. S. Ferreira, L. A. D. Carlos, *Sol. Energy Mater. Sol. Cells.* **2015**, *138*, 51.
[24] a) M. A. Cardoso, S. F. H. Correia, H. M. R. Gonçalves, R. F. P. Pereira, S. Pereira, T. M. R. Maria, M. M. Silva, A. J. M. Valente, E. Fortunato, R. A. S. Ferreira, V. de Zea Bermudez, *J. Sol-Gel Sci. Technol.* **2022**, *101*, 58; b) M. A. Cardoso, S. F. H. Correia, A. R. Frias, H. M. R. Gonçalves, R. F. P. Pereira, S. C. Nunes, M. Armand, P. S. André, V. de Zea Bermudez, R. A. S. Ferreira, *J. Rare Earth* **2020**, *38*, 531.
[25] B.-Y. Chang, S.-M. Park, *Annual. Rev. Anal. Chem.* **2010**, *3*, 207.
[26] M. M. Nolasco, P. M. Vaz, V. T. Freitas, P. P. Lima, P. S. André, R. A. S. Ferreira, P. D. Vaz, P. Ribeiro-Claro, L. D. Carlos, *J. Mater. Chem. A* **2013**, *1*, 7339.
[27] R. A. S. Ferreira, A. L. Ferreira, L. D. Carlos, *Eur. Phys. J. B* **2006**, *50*, 371.
[28] a) G. Atak, S. Ghorai, C. G. Granqvist, G. A. Niklasson, İ. Bayrak Pehlivan, *Sol. Energy Mater. Sol. Cells* **2023**, *250*, 112070; b) C. G. Granqvist, M. A. Arvizu, İ. Bayrak Pehlivan, H. Y. Qu, R. T. Wen, G. A. Niklasson, *Electrochim. Acta* **2018**, *259*, 1170; c) R. T. Wen, C. G. Granqvist, G. A. Niklasson, *Nat. Mater.* **2015**, *14*, 996.
[29] A. Eddahech, O. Briat, J.-M. Vinassa, *Electrochim. Acta* **2013**, *114*, 750.
[30] Z. Tong, J. Miao, J. Mao, Z. Wang, Y. Lu, *Energy Storage Mater.* **2022**, *50*, 533.
[31] L. Long, H. Ye, *Sci. Rep.* **2014**, *4*, 6427.
[32] A. Piccolo, F. Simone, *J. Build. Eng.* **2015**, *3*, 94.
[33] R. A. S. Ferreira, S. F. H. Correia, A. Monguzzi, X. Liu, F. Meinardi, *Mater. Today* **2020**, *33*, 105.
[34] M. C. Gonçalves, V. de Zea Bermudez, M. M. Silva, M. J. Smith, E. Morales, R. A. S. Ferreira, L. D. Carlos, *Ionics* **2010**, *16*, 193.
[35] S. J. Peakfit (Version 4.0) SYSTAT Software Inc.; 2007, CA, USA.
[36] a) D. H. Kaelble, K. C. Uy, *J. Adhes.* **1970**, *2*, 50; b) D. K. Owens, R. C. Wendt, *J. Appl. Polym. Sci.* **1969**, *13*, 1741.
[37] http://www.nanoscience.com/techniques/tensiometry/surface-tension-surface-free-energy-and-wettability/, **accessed March 2023**.

Manuscript received: September 19, 2023
Revised manuscript received: November 10, 2023
Version of record online: ■■, ■■

RESEARCH ARTICLE

Electrochromic windows: An electrochromic prototype incorporating a NIR-emitting hybrid electrolyte doped with an erbium complex and an ionic liquid provided a dual modulation operation suitable certain windows of buildings (*e.g.*, skylights, upper windows) located in cold climate regions. After 3-year storage at rest, the device demonstrated remarkable electro-optical performance enhancement, its figures of merit being competitive with current state-of-the-art values.

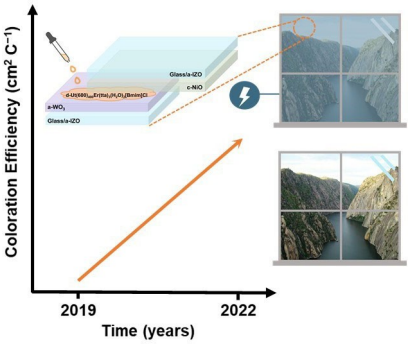

Dr. D. Pinheiro, Dr. M. Fernandes, Dr. R. F. P. Pereira, Dr. S. Pereira, Dr. S. F. H. Correia, Prof. Dr. M. M. Silva, Prof. Dr. E. Fortunato, Prof. Dr. R. A. S. Ferreira, Prof. Dr. M. C. Gonçalves, Prof. Dr. V. de Zea Bermudez**

1 – 13

NIR-emitting Electrochromic Windows for Cold Climate Region Buildings